crystals

MDPI

Article

Effect of Y on the Microstructures and Heat-Resistant Property of ZL109 Alloys

Xiangdu Qin [1], Anmin Li [1,2,3,*] and Xiang Li [1]

[1] School of Resources, Environment and Materials, Guangxi University, Nanning 530004, China; 15078266480@163.com (X.Q.); 15177617346@163.com (X.L.)
[2] State Key Laboratory of Featured Metal Materials and Life-Cycle Safety for Composite Structures, Guangxi University, Nanning 530004, China
[3] MOE Key Laboratory of New Processing Technology for Nonferrous Metals and Materials, Guangxi University, Nanning 530004, China
* Correspondence: lianmin@gxu.edu.cn

Abstract: The effects of rare earth Y on the microstructures and tensile properties of ZL109 alloys were studied through metallographic observation, scanning electron microanalysis, X-ray diffraction, and tensile experiments, and the existence form and mechanism of Y were analyzed. The results show that the grain size of the ZL109 alloy is obviously reduced and that the strength of the ZL109 alloy is significantly increased after adding the Y element. When the Y content is increased to 0.2 wt.%, the tensile properties of the ZL109 alloy at room temperature and 350 °C are better than those without a rare earth addition, and the comprehensive tensile properties are better. This is due to the addition of the Y element; α-Al dendrites are obviously refined, and there is a tendency for them to change into fine isometric crystals. The size of the eutectic Si decreases, and its shape is modified. The morphology and size of high temperature enhanced phases, such as Al_3CuNi, are optimized. The heat-resistant enhanced phase Al_2Si_2Y is formed after the addition of rare earth Y. However, with the addition of the Y element, the Al_2Si_2Y phase increases, and coarsening results in the decrease in alloy strength.

Keywords: ZL109; Y; heat-resistant property

Academic Editor: Heinz-Günter Brokmeier

Received: 20 December 2024
Revised: 3 January 2025
Accepted: 11 January 2025
Published: 14 January 2025

Citation: Qin, X.; Li, A.; Li, X. Effect of Y on the Microstructures and Heat-Resistant Property of ZL109 Alloys. *Crystals* **2025**, *15*, 75. https://doi.org/10.3390/cryst15010075

1. Introduction

Due to their excellent specific strength and low density, aluminum alloys are gradually replacing traditional steel materials in automotive parts and other applications [1]. However, components made of aluminum alloys tend to significantly decrease their high temperature mechanical properties due to the growth of their grains and precipitates at high temperatures, thus making them unusable in high temperature environments [2]. The development of cast heat-resistant aluminum alloys that can be used safely for a long time in the temperature range of 300 to 400 °C has become an international research hotspot in recent years [3].

A cast heat-resistant aluminum alloy refers to an aluminum alloy prepared by casting, served at 150 to 350 °C, with sufficient oxidation resistance, and under the long-term action of heat-force coupling, with certain creep resistance and mechanical properties [4]. Cast heat-resistant aluminum alloys can be roughly divided into an Al-Si series, an Al-Cu series, and an Al-Mg series of cast heat-resistant aluminum alloys. The Al-Si cast heat-resistant aluminum alloy is the most used and widely used cast heat-resistant aluminum alloy at present, and its output and application amount account for more than 90% of the total cast

heat-resistant aluminum alloys [5]. Due to the presence of Si elements, A1-Si alloys have good air tightness, fluidity, small casting shrinkage, and other casting properties, and they can be widely used in the pistons and cylinders of automotive engines [6]. However, the plastic toughness of the Al-Si alloy is still relatively poor, and the mass fraction of Si in industrial production is generally between 4 and 22 wt.%. The heat resistance strengthening phase is often formed by adding Cu, Ni, Mg, Mn and other elements to improve the mechanical properties of the alloy [7]. Al-Si cast heat-resistant aluminum alloys can be divided into Al-Si-Mg, Al-Si-Cu, and Al-Si-Cu-Mg-Ni [8]. The strength of the Al-Si-Mg alloy is improved mainly by the Mg_2Si strengthening phase, but the properties of the Al-Si-Mg alloy decrease rapidly due to the obvious coarsening during the Mg2Si phase at high temperature [9]. The Al-Si-Cu alloy relies on the θ-Al_2Cu phase and the Q-$Al_5Cu_2Mg_8Si_6$ phase to play a strengthening role, but the high temperature stability of the θ-Al_2Cu phase and the Q-$Al_5Cu_2Mg_8Si_6$ phase will also decline sharply when the temperature exceeds 200 °C and 250 °C [10]. Studies have shown that after adding Ni elements to the Al-Si-Cu-Mg alloy, Ni-rich strengthening phases, such as Al_3CuNi, Al_3Ni, and Al_7Cu_4Ni, will be formed in the alloy, which can significantly improve the high temperature performance of the alloy above 300 °C [11]. Therefore, the research of casting an Al-Si-Cu-Mg-Ni heat-resistant aluminum alloy that can meet the more severe high temperature environment will make the goal of achieving lightweight automobiles using aluminum instead of steel one step closer. Among these alloys, the Al-Si-Cu-Mg-Ni series ZL109 heat-resistant aluminum alloy, independently developed by China, is still the most widely used piston alloy material in China. Selection of the ZL109 alloy as the matrix alloy that is to be used to cast a heat-resistant aluminum alloy with higher performance is the objective of this study.

The addition of Ni, Ag [12], Mn [13], Zr [14], and other transition metal elements and rare earth elements such as Sc [15], La [16], and Y [17] for the basis of casting the Al-Si-Cu-Mg aluminum alloy can reduce the layer fault energy of the alloy system and form a high temperature stable heat-resistant phase and a nanometer coherent precipitated phase. Pinning dislocations and blocking grain boundary movement at high temperatures are effective ways to improve heat resistance. Abhishek et al. [12] studied the effects of trace amounts of Ag and Sn elements on the precipitates and mechanical properties of the 7075 alloy and showed that adding a small amount of Ag and Sn to the 7075 alloy could significantly reduce the average grain size of the alloy. Ag and Sn reduce the formation of coarse η precipitates by trapping quenched vacancies and reducing the concentration of free vacancies. Ag and Sn accelerate the kinetic rate of the precipitated phase, and all phase transitions are controlled by the dynamics of Ag and Sn. After adding Ag and Sn, the strength and ductility of the 7075 alloy are significantly improved. Jun et al. [14] studied the effect of Zr on the microstructure and mechanical properties of the Al-Si-Cu-Mg alloy at intermediate temperature (100–200 °C). It was found that Zr can effectively inhibit the nucleation and grain growth of the alloy and refine the grain. The size of the eutectic Si and Fe-rich phase of the alloy decreased significantly. The highest intermediate temperature thermal exposure performance (150 °C/20 h) was obtained by adding 0.2% Zr, and the tensile strength and elongation were 208.1 MPa and 11.4%, respectively, which were significantly better than those without Zr. Rare earth elements have good chemical activity and can form intermetallic compounds with other elements in the alloy. It Zr promotes heterogeneous nucleation, which allows the thinning of α-Al dendrites [18]. The microstructure optimization of the Al-Si alloy can be divided into three parts, namely, eutectic silicon refining, primary silicon refining, and α-Al refining. Li [19] systematically studied the influences of the Y element on the morphology and size of α-Al, primary Si, and eutectic Si in the multi-component eutectic Al-13Si-3Cu-2Ni-0.5Mg alloy. When the addition of rare earth Y is 0.8%, the coarse α-Al dendrites in the alloy are refined into

uniform cellular or equiaxial crystals, and the secondary dendrite arm spacing decreases from 12.7 μm to 4.5 μm—a decrease of 64.6%. The coarse lamellar or long acicular eutectic Si is transformed into a fine fibrous structure with many branches. The tensile properties of an as-cast Al-13Si-3Cu-2Ni-0.5Mg alloy at room temperature and at high temperature are also significantly improved. Yu et al. [20] explored the effect of Y on the microstructure and mechanical properties of the ZL107 alloy at room temperature. When the content of Y was equal to or greater than 0.1 wt.%, the eutectic Si was completely modified, and the shape of the eutectic Si became short rod or granular. With the further increase in the Y content, the shape of the eutectic Si does not change. After adding 0.1 wt.% Y, the tensile strength increased from 194.3 MPa to 203.4 MPa, and the elongation increased from 2.3% to 2.6%. The tensile strength and elongation decreased with the increase in the Y content. In addition, some studies have shown that rare earth Y and the aluminum form rare earth phase Al_3Y, which prevents grain growth and grain boundary slip at high temperature, plays a role in grain boundary strengthening, and can improve the high temperature strength of aluminum alloys [21].

At present, there are many studies on the modification and refinement of rare earth Y in casting Al-Si alloys, and most of them focus on the mechanical properties at room temperature. However, the effect of rare earth Y on the strengthening phase in the Al-Si-Cu-Mg-Ni alloy and its mechanism still need further experimental investigation. The study of high temperature properties in this paper has certain novelty. The aims of this study are to optimize a cast heat-resistant aluminum alloy on the basis of the existing ZL109 alloy, so that the optimized alloy has better room temperature and high temperature properties than the ZL109 alloy, and to analyze the existence form of rare earth Y in the Al-Si-Cu-Mg-Ni alloy and the strengthening mechanism of rare earth Y on the ZL109 alloy.

2. Materials and Methods

In the experiment, the ZL109 piston alloy was used as the base alloy, and different contents of the Y element were added to form 5 control groups. The nominal chemical compositions and the measured actual chemical compositions of the alloys are shown in Tables 1 and 2, respectively. The raw materials used in the experiment are industrial high-pure aluminum blocks (99.90%), Al-50Si, Al-50Cu, Al-20Mg, Al-20Ni and Al-10Y intermediate alloys produced by Haichuan Metal Materials Co., Ltd. (Suzhou, China).

Table 1. The nominal chemical compositions of ZL109-xY alloys (wt.%).

Alloy	Si	Cu	Mg	Ni	Y	Al
Y-free	12	1.2	1.2	1.2	0	Bal.
2Y	12	1.2	1.2	1.2	0.2	Bal.
4Y	12	1.2	1.2	1.2	0.4	Bal.
6Y	12	1.2	1.2	1.2	0.6	Bal.
8Y	12	1.2	1.2	1.2	0.8	Bal.

Table 2. The actual compositions of ZL109-xY alloys (wt.%).

Alloy	Si	Cu	Mg	Ni	Y	Al
Y-free	12.13	1.18	1.22	1.21	0	Bal.
2Y	12.25	1.21	1.19	1.22	0.21	Bal.
4Y	11.98	1.23	1.23	1.18	0.37	Bal.
6Y	11.93	1.17	1.17	1.23	0.59	Bal.
8Y	12.07	1.23	1.18	1.18	0.78	Bal.

First, the pure aluminum ingot and graphite crucible together were put into a well resistance furnace. The furnace was heated to about 800 °C, and then the required intermediate alloys were added in turn. The covering agent was added, and the melt was left to keep warm for 10 min; then, the melt was stirred and slagged. When the furnace temperature dropped to about 680–700 °C, the Mg patch was quickly pressed into the bottom of the solution, held for 5 min, and refined; then, the power was adjusted again to make the furnace temperature rise to 710 °C for mechanical stirring for 2 min. After being degassed by C_2Cl_6, the melt was cast into a preheated steel mold at around 730 °C. The heat treatment process used for the samples was a T6 heat treatment: after the samples were held at 505 °C for 6 h, they were quenched with hot water at 70–90 °C, and then the cooled samples were held at 180 °C for 6 h. Subsequently, the samples were taken out for air cooling. After that, the alloy samples were etched with Keller's reagent (1% HF + 1.5% HCl + 2.5% HNO_3 + 95% H_2O). An X-ray diffractometer (Rigaku D/MAX 2500V, Rigaku Corporation, Akishima, Japan), a metallographic microscope (BH200M, Sunyu Instrument Corporation, Ningbo, Chian), a field emission scanning electron microscope (Sigma 300, ZEISS, Oberkochen, Germany), and an EDS (S3400N, Hitachi Corporation, Tokyo, Japan, accelerating voltage, 20 KV) were used to characterize the microstructures and phase analysis of the samples. Elemental analysis of the samples was performed using an X-ray fluorescence element analyzer (S8 TIGER, BRUKER, Berlin, Germany). The tensile properties of the series of alloys at room temperature were performed on a universal testing machine (AGS-X 100KN, Shimadzu, Shanghai, China) with a standard drawing distance of 25 mm and a drawing rate of 0.5 mm/min. The high temperature mechanical properties were performed on a testing machine (Kappa, ZWICK, Ulm, Germany) at a tensile rate of 0.5 mm/min.

3. Results and Discussion

3.1. Microstructure of Alloys

Figure 1 shows the XRD results of the ZL109 alloys with different Y content. It can be found that the alloys consist of α-Al, a eutectic Si phase, an Al_3Ni phase, an Al_3CuNi phase, a Mg_2Si phase, and a small amount of Al_2Cu. However, the $Al_5Cu_2Mg_8Si_6$, Al_7Cu_4Ni, and other possible second phases were not found. No new diffraction peak appeared after the Y element was added, and no phase containing Y was found. The XRD results were correlated with the content of each component phase. Because some alloying elements are solidly dissolved in an Al matrix and the alloying phase content is small, the corresponding diffraction peak is not found in the back of the diffraction pattern. The existence form of rare earth Y in the ZL109 aluminum alloy and the type and variation of the strengthening phase in the alloy need to be further analyzed based on the SEM–EDS results.

As can be found from Figure 2, the alloy structure is primarily composed of primary Al and eutectic Si. According to the results of the metallographic microstructures and phase analysis, the most abundant light-colored phase is the α-Al matrix with continuous distribution. The black phase is mostly a spherical and rod-like eutectic Si phase, and only contains a small amount of the irregular bulk primary Si phase. A small amount of light gray intermetallic compounds is also observed. After the Y element is added to the matrix alloy, the α-Al structure is further refined and tends to change to fine isometric crystals. With the increase in the Y content, the eutectic Si becomes more rounded and changes from a short rod-like to a spherical shape, indicating that Y has a significant modification effect on the eutectic Si, which is consistent with the research results of Li [22] et al. The Si phase and the intermetallic compounds are mainly concentrated in the dendrites, and small amounts are distributed in the crystals. In view of the metamorphic mechanism of the eutectic Si, some researchers have proposed that the ideal ratio of the atomic radius of

the metamorphic element to the atomic radius of silicon is about 1.65 [23]. The r_Y/r_{Si} value of 1.55 is close to the ideal value; therefore, the Y element has an obvious metamorphic effect on the eutectic Si, and the size of the eutectic Si is obviously refined.

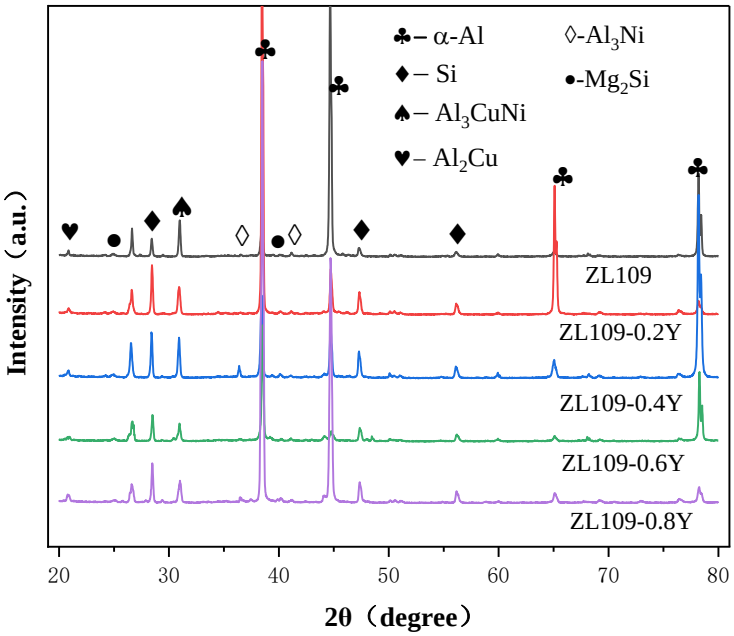

Figure 1. X-ray diffraction patterns of ZL109-xY alloys.

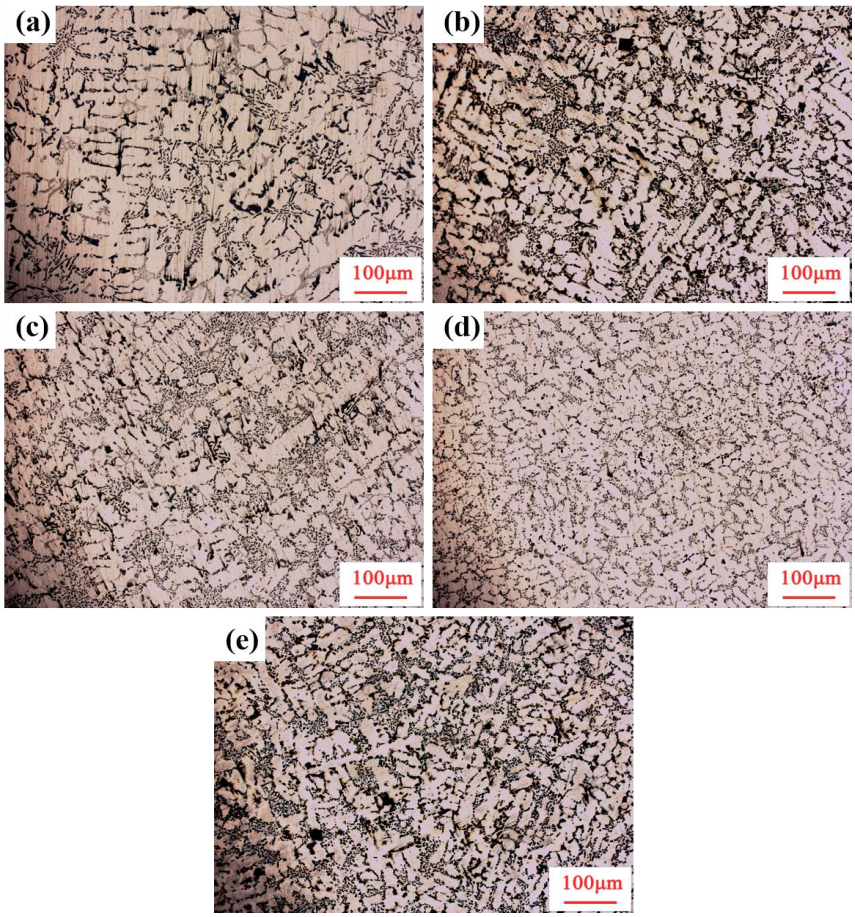

Figure 2. Effect of different Y additions on microstructures of ZL109-xY alloys: (**a**) Y-free; (**b**) 0.2Y; (**c**) 0.4Y; (**d**) 0.6Y; and (**e**) 0.8Y.

In order to explore the metamorphism of the Y element on the eutectic Si, the Image J 2024 software was used to measure and analyze the size and form factor of the eutectic Si alloy particles, and the results are shown in Figure 3. The size of the eutectic Si decreases with the increase in the Y content. When the Y content increases to 0.6 wt.%, the size of the eutectic Si is basically unchanged by adding the Y element. When the Y content is 0.8 wt.%, the minimum average size is 3.58 μm. Form factor, also known as roundness [24], is the aspect ratio of the eutectic Si particles, and the test results are basically consistent with the size change rule. When the Y content is 0.6 wt.%, the form factor is closest to 1, and the form factor increases slightly with the addition of the Y element.

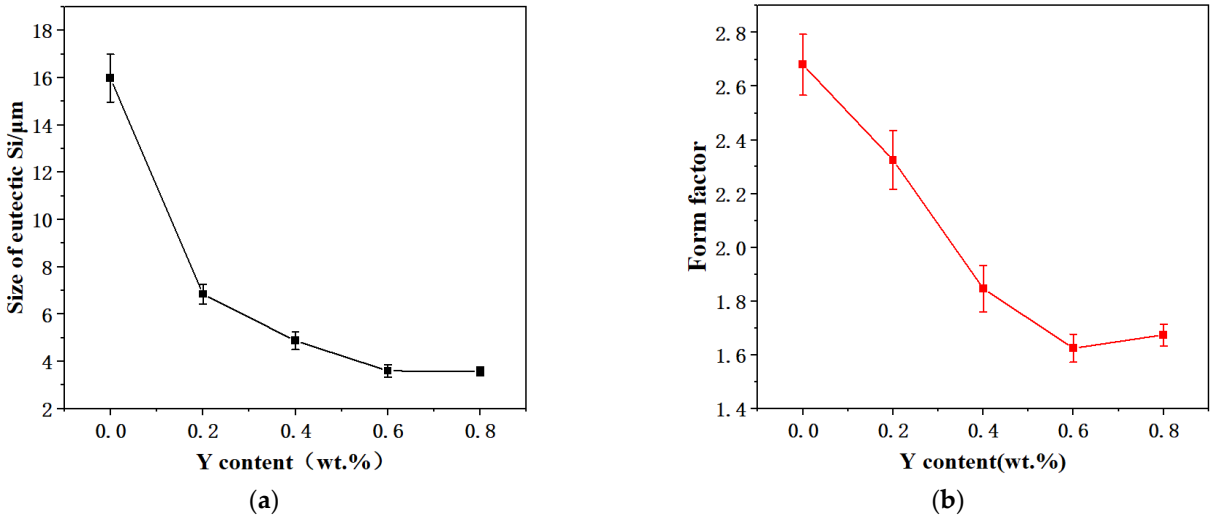

Figure 3. (**a**) Eutectic Si size of ZL109-xY alloys; (**b**) Form factor of eutectic Si in ZL109-xY alloys.

Figure 4 shows the SEM morphology of the ZL109-0Y alloy. According to the EDS results (as shown in Figure 6), it was determined that the strip structure is the Al_3Ni phase, the network or Chinese character is the Al_3CuNi phase, and the black microstructure is the Mg_2Si phase. However, the Al_2Cu may not have been detected due to its small content and relatively small size.

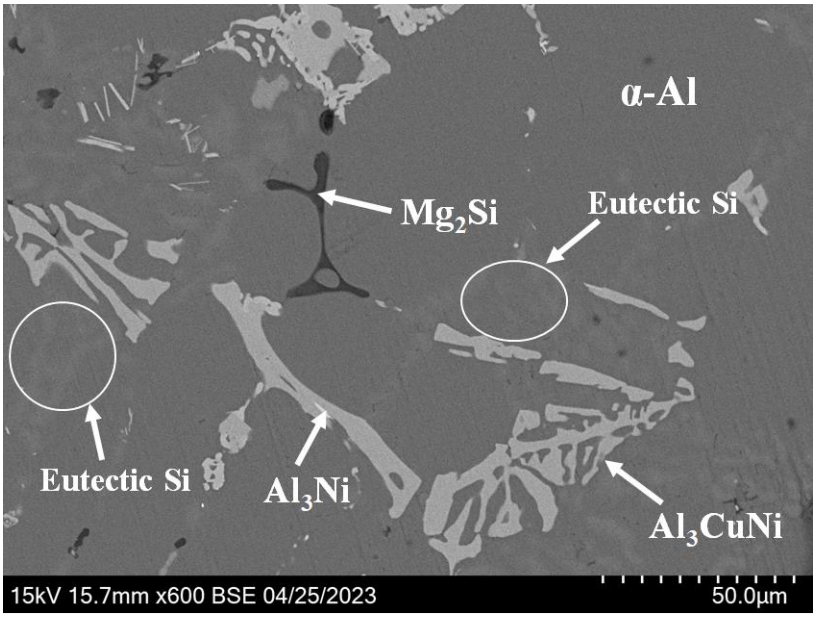

Figure 4. SEM microstructure of ZL109-0Y alloy.

The microstructures of the ZL109 alloys with different Y content are shown in Figure 5. It can be found from the figure that after the Y element is added, the brighter Ni-rich phase in the alloy is striped and radial, and the size is significantly reduced. The average size of the Ni-rich phase in the ZL109-0Y, ZL109-0.2Y, ZL109-0.4Y, ZL109-0.6Y, and ZL109-0.8Y alloys is 28.61 μm, 12.69 μm, 14.80 μm, 15.56 μm, and 17.79 μm, respectively. The Ni-rich phase decreased significantly after the Y element was added. Moreover, according to the surface scanning energy spectrum results of the ZL109-0.6Y alloy (as shown in Figure 6), the Y element is enriched in the Ni-rich phase and the eutectic Si phase, and is less distributed in the Al matrix. With the increase in the Y content, the thinning effect of the Y element is weakened, and the coarsening phenomenon of the Ni-rich phase is obvious.

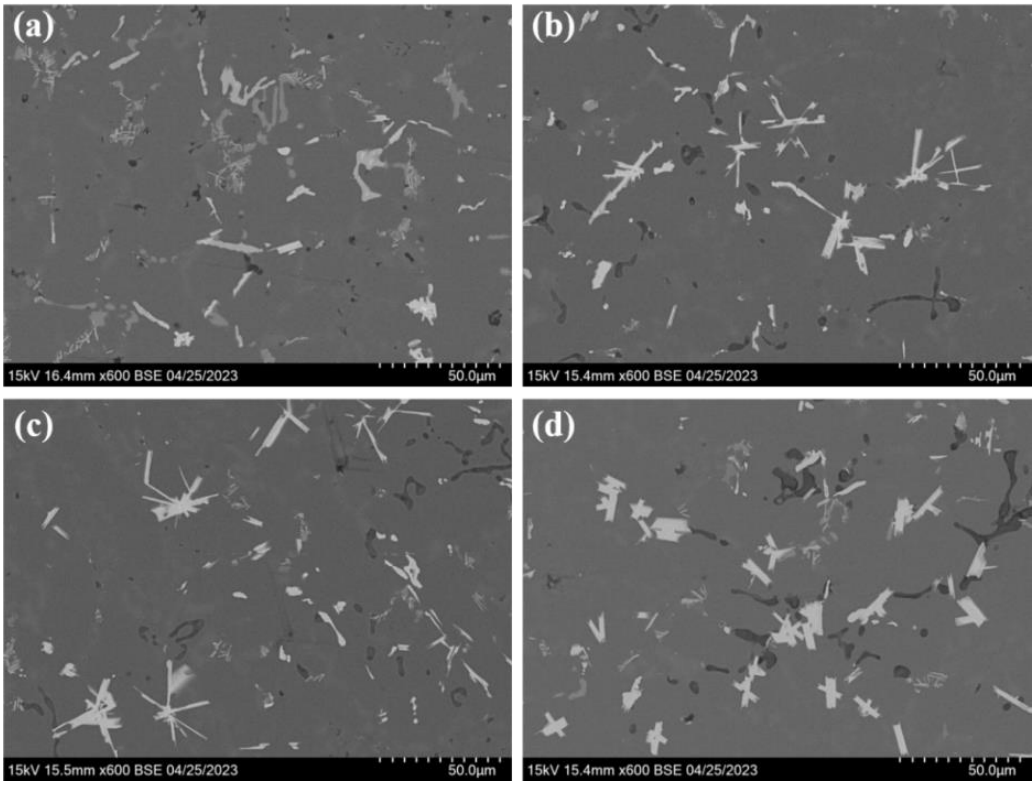

Figure 5. SEM microstructures of ZL109-xY alloys: (**a**) 0.2Y; (**b**) 0.4Y; (**c**) 0.6Y; and (**d**) 0.8Y.

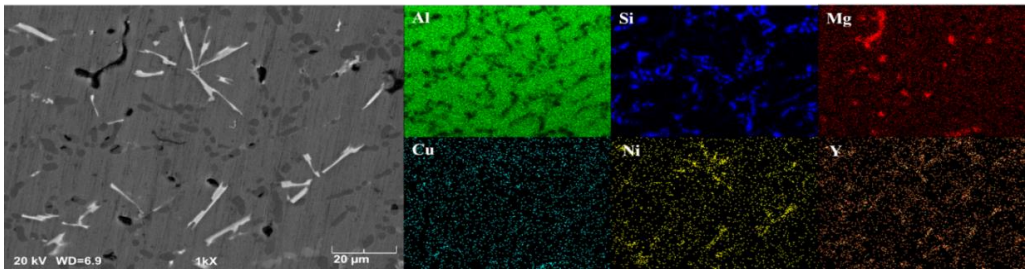

Figure 6. SEM microstructure of ZL109-0.4Y alloy.

In order to further determine the existence form of the Y element in the alloy, the microstructures of the ZL109-xY (x = 0.4, 0.8) alloys were analyzed. The SEM topography and point analysis results are shown in Figure 7 and Table 3, respectively. According to the results, the Ni-rich phase is mainly the Al_3CuNi phase, and the Y element tends to form the Al, Si, Ni, Y multi-component phase; that is, there are two closely combined phases—an Al_3Ni phase and a yttrium-rich phase—that are difficult to distinguish. Figure 7b shows that when the Y content is 0.8 wt.%, the morphology of the Al_3CuNi phase changes significantly,

and these phases always attach to the compound phase. The energy spectrum results of Spot 4 and Spot 5 in Figure 7b show that the atom ratio of silicon yttrium is close to 2:1, no Cu is detected, and a small amount of Mg is contained—which is basically consistent with the energy spectrum results of the Al_2Si_2Y phase reported by Wan [25] et al. Therefore, it is speculated that the existing Y-rich phase is the Al_2Si_2Y phase. The existence of the Al_3Ni phase is confirmed by the XRD phase analysis; therefore, it is further proved that the Al_3Ni phase and the Al_2Si_2Y phase coexist And that Al_2Si_2Y can inhibit dislocation and grain boundary movement and improve the mechanical properties of the aluminum alloy [25].

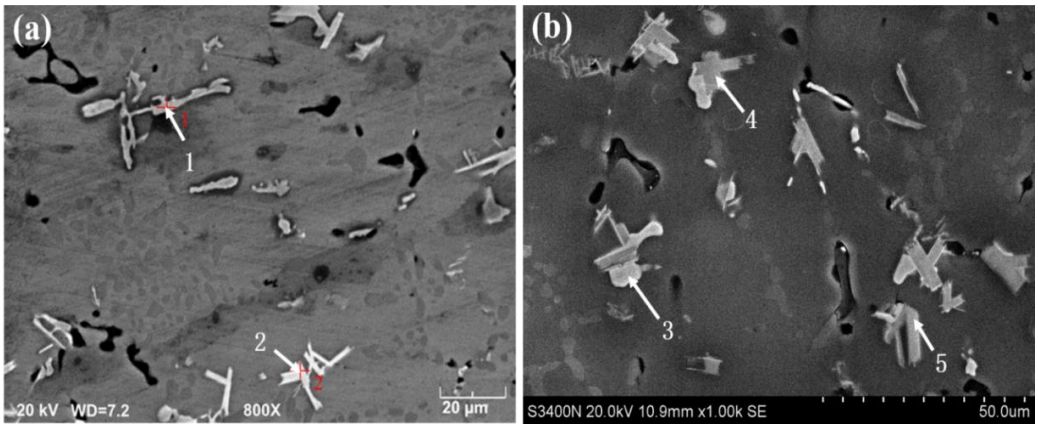

Figure 7. SEM microstructures of ZL109-xY alloys: (**a**) 0.4Y and (**b**) 0.8Y.

Table 3. EDS analysis is of phases at locations depicted in Figure 2 (wt.%).

Spot	Al	Cu	Ni	Si	Mg	Y	Phase
1	45.681	23.222	27.369	2.010	0.869	0.264	Al_3CuNi
2	41.491	1.395	20.179	15.538	1.079	17.468	Al_3Ni, Al_2Si_2Y
3	70.728	13.289	14.543	0.000	1.440	0.000	Al_3CuNi
4	52.130	0.505	8.710	24.521	2.338	11.796	Al_3Ni, Al_2Si_3Y
5	50.528	0.424	7.787	26.346	2.112	12.802	Al_2Si_2Y

3.2. Tensile Properties of Alloys

The relationship between yield strength and grain size of metallic materials can be expressed by the Hall–Petch equation (as shown in Equation (1) [26]). In the formula, σ_s is the yield stress of the material, σ_0 represents the constant of the initial stress of dislocation motion, k represents the strengthening coefficient, and d represents the average grain diameter.

$$\sigma_s = \sigma_0 + kd^{-\frac{1}{2}} \quad (1)$$

Figure 8 and Table 4 show the tensile strength, yield strength, and elongation of the ZL109-xY alloys at room temperature. The relevant data of tensile test performance of the ZL109-xY alloys at room temperature are shown in Table 4. By comparing the ZL109-xY alloys, it can be found that with the increase in the Y content, the tensile strength of the ZL109-xY alloys at room temperature first increases and then decreases. When the Y content is increased to 0.2 wt.%, the tensile strength of the alloys is increased from 273.73 MPa to 313.08 MPa by 14.4%, and the comprehensive tensile property is better. However, with the addition of the Y element, the tensile strength and plasticity of the alloys decrease.

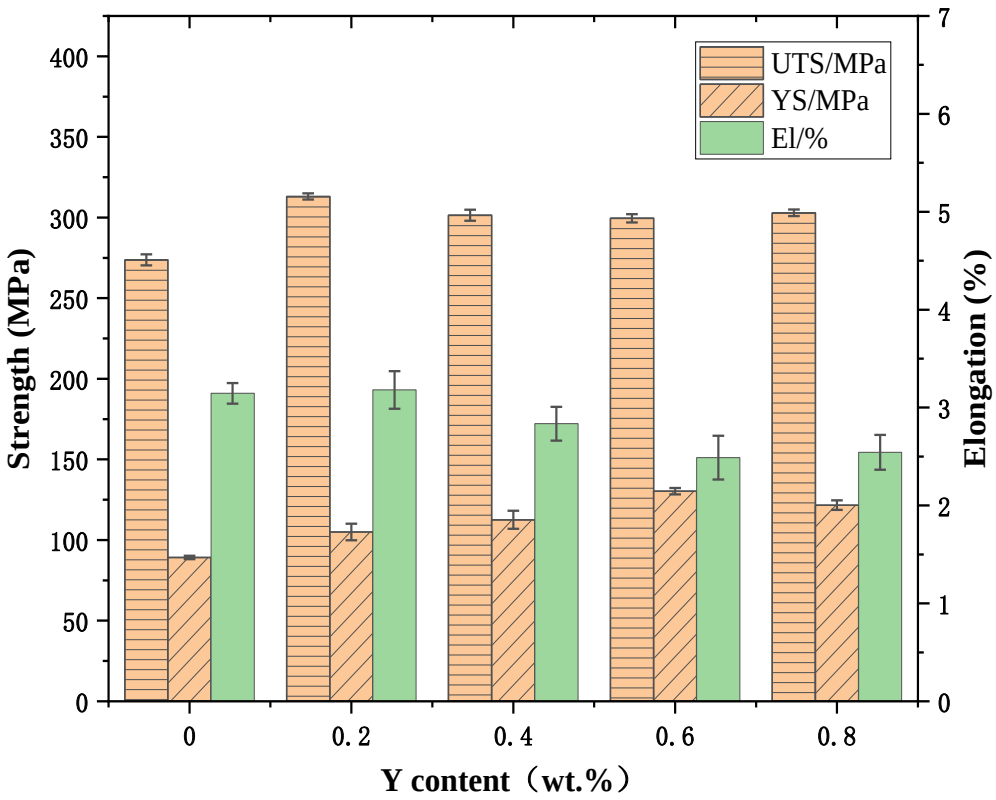

Figure 8. Tensile strength, yield strength, and elongation of ZL09-xY alloys with different Y content at room temperature.

Table 4. Relevant tensile test data of ZL109-xY alloys at room temperature.

Y (wt.%)	Tensile Strength (MPa)	Yield Strength (MPa)	Elongation (%)
0	273.73	89.14	3.15
0.2	313.08	105	3.18
0.4	301.43	112.56	2.84
0.6	299.52	130.3	2.49
0.8	302.91	121.63	2.54

Under the combined action of the Y element and the strengthening phase, the ZL109-0.2Y alloy has good mechanical properties at room temperature. However, according to relevant studies and the analysis of the Griffith crack theory, the thick and slender eutectic Si particles are more prone to fracture. With the increase in the Y content, Si particle size decreases, and the critical stress of crack instability propagation increases [27]. Smooth spherical eutectic Si greatly reduces stress concentration, and the strength and plasticity of the alloy should be significantly improved. However, with the addition of the Y element, the tensile strength and plasticity of the alloy decrease. Griffith's formula [28] is shown in Equation (2): σ_c is the critical stress for the unstable propagation of a crack in the Si phase; E is the elastic modulus of the Si phase; γ_s is the specific surface energy of the Si phase crack; a is the half-length of the Si phase crack.

$$\sigma_c = \left(\frac{2E\gamma_s}{\pi a}\right)^{\frac{1}{2}} \quad (2)$$

In order to investigate the reason for the plasticity decline, the fracture of the tensile specimen at room temperature was further analyzed. Figure 9 shows the tensile fracture

SEM morphologies of the ZL109 alloys with different the Y content at room temperature. The fractures are mainly composed of a cleavage plane—a large number of short and curved tearing edges and quasi-cleavage facets that are characterized by cleavage and quasi-cleavage—and are typical brittle fractures [28–30], consistent with the result of low elongation and poor plasticity after fracture. At the same time, it can be seen that there are a large number of micro-cracks in the fracture and that the quasi-cleavage fracture is a discontinuous fracture, with each hidden small crack growing constantly; this connection often has a large plastic deformation, thus forming tearing edges and quasi-cleavage facets [28–30].

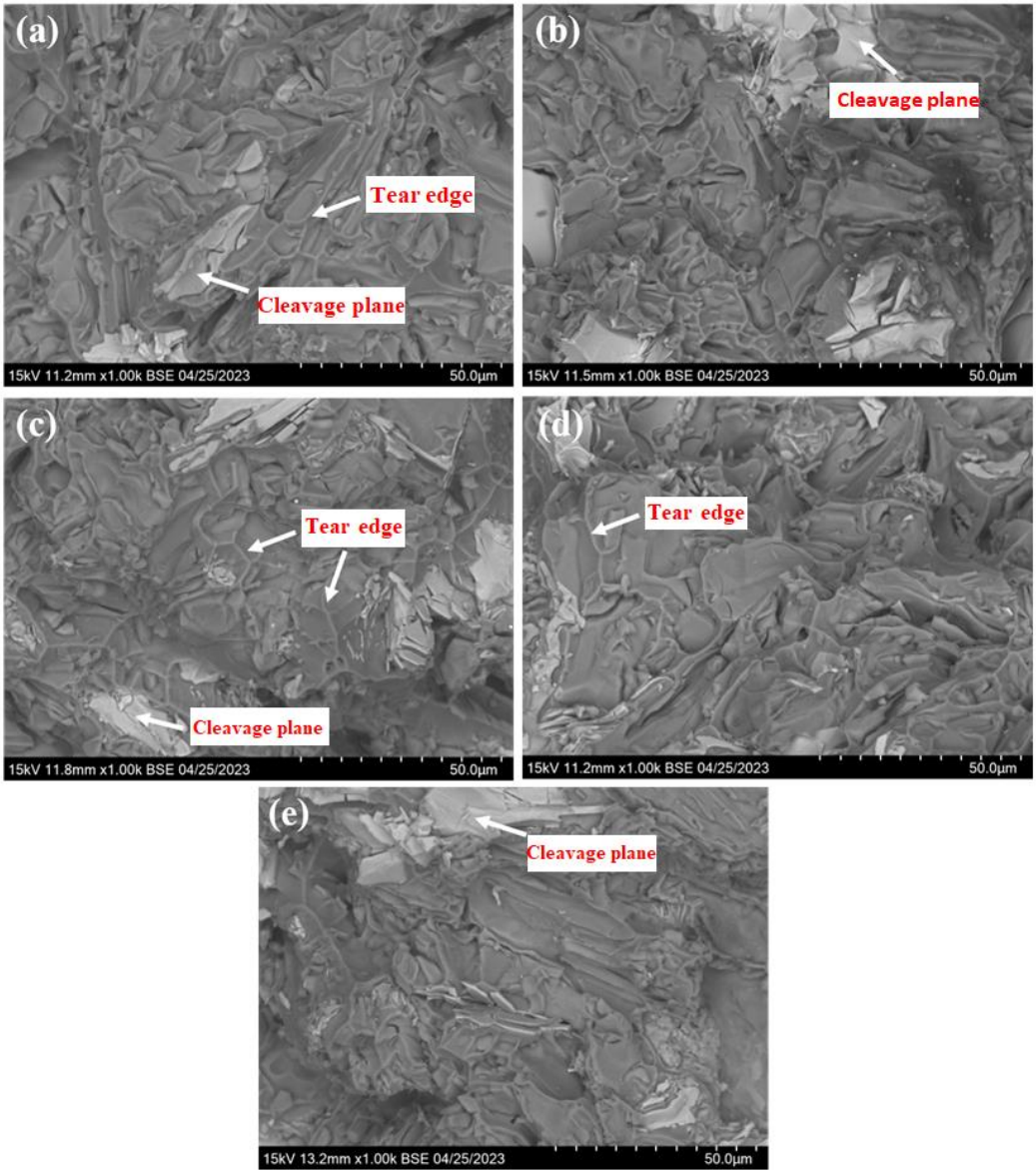

Figure 9. Tensile fracture morphologies of ZL109-xY alloys at room temperature: (**a**) 0Y; (**b**) 0.2Y; (**c**) 0.4Y; (**d**) 0.6Y; and (**e**) 0.8Y.

In order to further explore the causes of plastic decline and fracture sources of the alloy, energy spectrum analysis was also carried out on the tensile fracture structure of the ZL109-0.6Y alloy at room temperature, and the results are shown in Figure 10. There are micro-cracks in one convex structure and two sections formed by the quasi-cleavage fracture, which belong to the fracture source. At the same time, according to the point analysis results, the fracture source is the Al_3Ni phase and the Al_2Si_2Y phase. The results

show that with the increase in the Y content, the Al_2Si_2Y phase content and coarsening are more likely to crack, reducing the mechanical properties of the alloy.

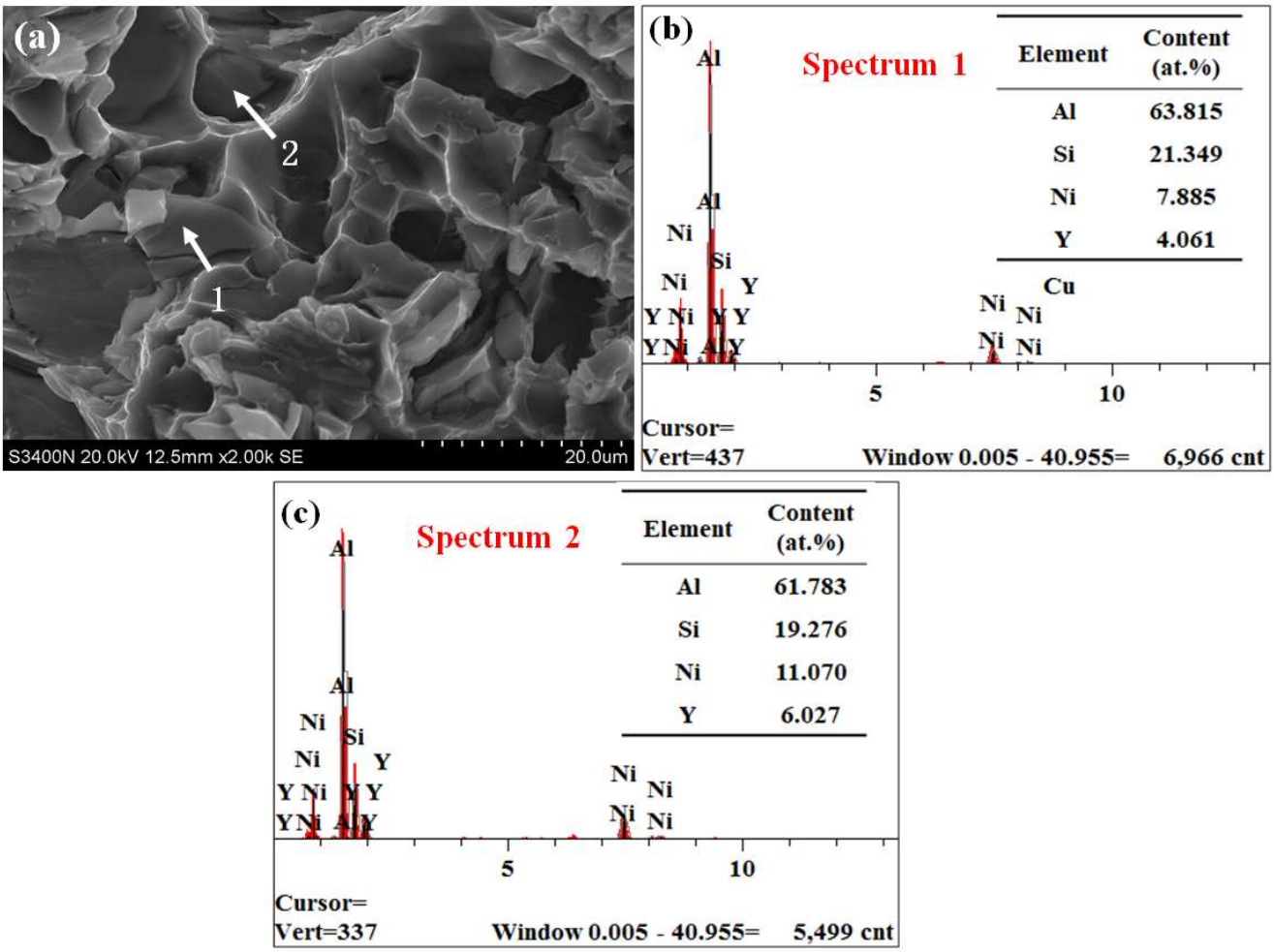

Figure 10. (**a**) Tensile fracture morphology of ZL109-0.6Y alloy; (**b**) EDS data at point 1; (**c**) EDS data at point 2.

3.3. Test Results and Analysis of Tensile Properties of Alloys at High Temperature

The tensile test results of the ZL109-xY alloys at high temperature (350 °C) are shown in Figure 11 and Table 5. The results show that the tensile strength at high temperature increases first and then decreases with the increase in the Y content. The high temperature tensile strength and yield strength of the ZL109-0.2y alloy are the highest, which are increased by 17.4% and 18.9%, respectively, compared with the ZL109 alloy. With the increase in the Y content, the elongation of the alloy shows an increasing trend. The results show that the second phase strengthening is the main strengthening mechanism under high temperature conditions, and the alloy strength is related to the shape, size and distribution of the second phase thermal stability [31]. Combined with the above results, it can be seen that when the Y content is 0.2%, the size of the Ni-rich phase is the smallest and the distribution is uniform, so the ZL109-0.2Y alloy has the best tensile strength. The addition of rare earth Y led to the coarsening of the Ni-rich phase and the Y-rich phase, which led to the decrease in the high temperature strength of the alloy. At the high temperature of 350 °C, the grain boundary strength decreases, the hindering effect on dislocation decreases, and the grain boundary slip is easier to carry out [32]. Combined with the above results, it can be seen that the size of the eutectic silicon and α-Al decreases with the increase in the Y

content. This forms more grain boundaries, making the alloy more plastic; therefore, the elongation increases. This result is consistent with the experimental results of Yang [32].

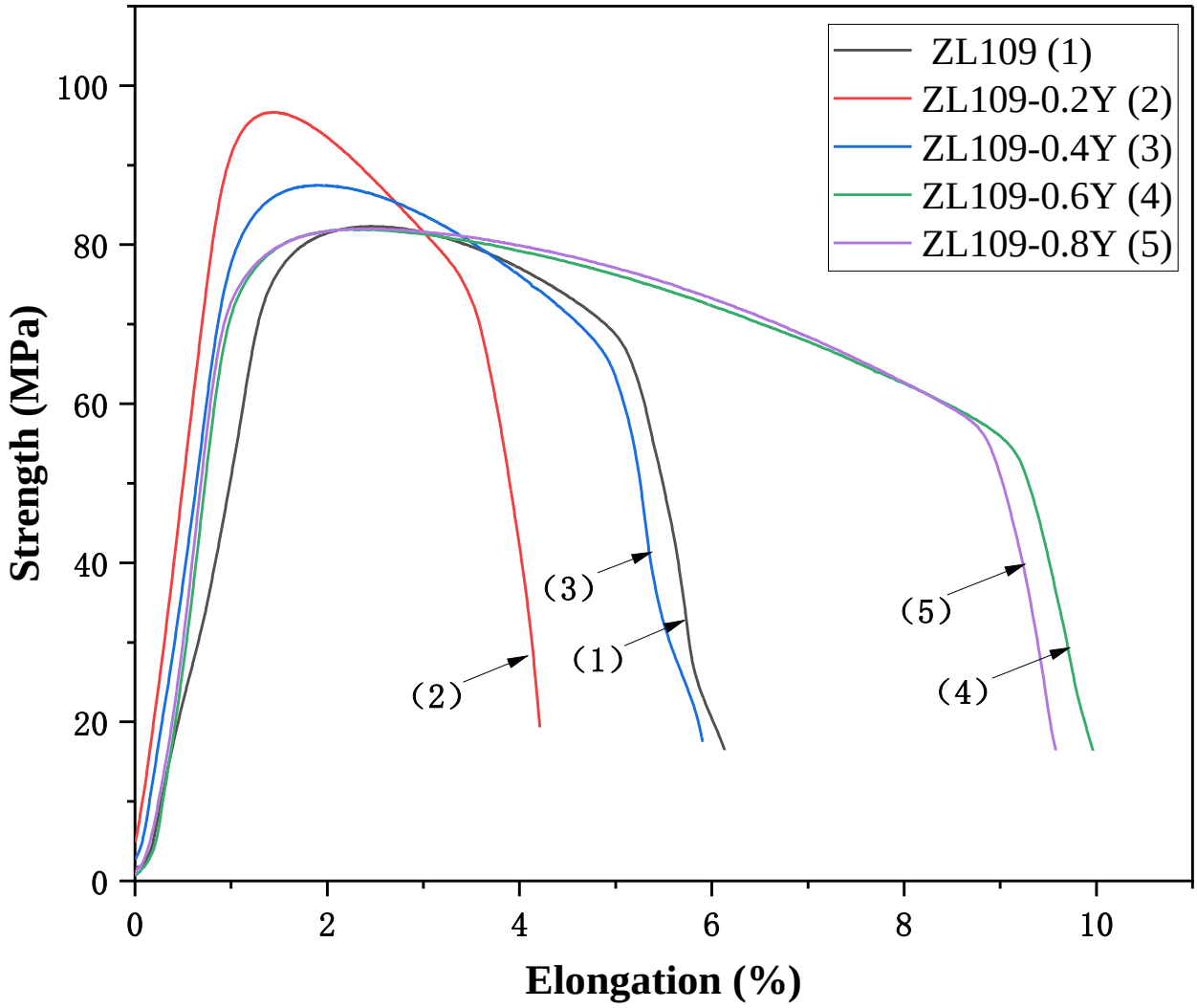

Figure 11. Tensile properties of ZL109-xY alloys at high temperature (350 °C).

Table 5. Relevant tensile test data of ZL109-xY alloys at high temperature (350 °C).

Y (wt.%)	Tensile Strength (MPa)	Yield Strength (MPa)	Elongation (%)
0	82.3	78.71	5.21
0.2	96.65	93.62	3.66
0.4	87.48	81.34	5.14
0.6	81.94	75.77	8.76
0.8	82	77.1	8.62

Figure 12 shows the SEM morphology of tensile fractures of the ZL109 alloys with different Y content at room temperature. Compared with the tensile fracture at room temperature, the tensile fracture at high temperature mainly has two kinds of micromorphologies: equiaxial dimple and tear edge, and there are a few cleavage planes, which belong to the mixed ductile and brittle fracture. Figure 12b shows the tensile fracture morphology of the alloy with a Y content of 0.2 wt.% at high temperature. The number of isometric dimples is relatively small, and there are more tearing edges in the fracture. Therefore, the ZL109-0.2Y alloy shows the worst plasticity. With the increase in the Y

content, the number of isometric dimples increases, and the plasticity of the alloy increases gradually [28–30].

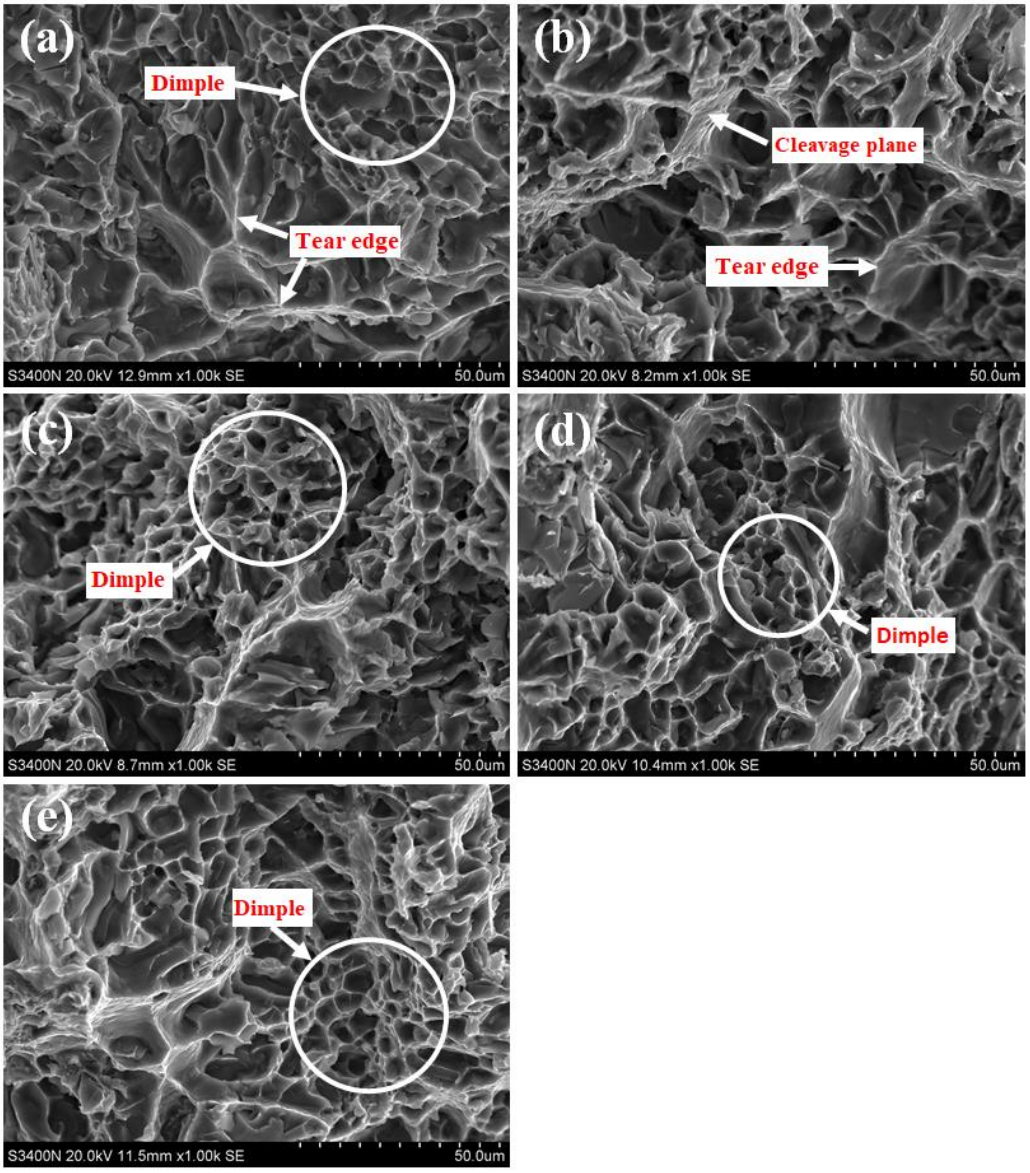

Figure 12. Tensile fracture morphologies of ZL109-xY alloys at high temperature (350 °C): (**a**) 0Y; (**b**) 0.2Y; (**c**) 0.4Y; (**d**) 0.6Y; and (**e**) 0.8Y.

4. Conclusions

In this paper, the microstructures and tensile properties of the ZL109-xY (x = 0.2, 0.4, 0.6, 0.8, wt.%) series alloys were analyzed; the existence form of rare earth Y in the ZL109 aluminum alloy was explored; and the influence of the Y element on the tensile properties of the alloy was analyzed, along with the strengthening mechanism of the alloy. The conclusion is as follows:

(1) The strengthening phases of the ZL109-xY alloy include the eutectic Si phase, the Al_3Ni phase, the Al_3CuNi phase, the Al_2Si_2Y phase, the Mg_2Si phase, and a small amount of the Al_2Cu phase; moreover, the Al_3Ni phase and the Al_2Si_2Y phase always exist simultaneously.

(2) The tensile strength of the ZL109-xY alloy at room temperature and at high temperature increases first and then decreases with the increase in the Y content. When the Y content is 0.2 wt.%, the tensile strength of the alloy at room temperature is 313.08 MPa,

which is 14.4% higher than that of the ZL109 alloy, and the comprehensive tensile property is better. The tensile strength and the yield strength of the ZL109-0.2Y alloy at high temperature are the highest, which are increased by 17.4% and 18.9%, respectively, compared with the ZL109 alloy. Therefore, the ZL109-0.2Y alloy has the better comprehensive mechanical properties.

(3) The strengthening phase Al_2Si_2Y is formed by adding the Y element to the ZL109 alloy, which can inhibit dislocation and grain boundary movement. The α-Al dendrites are obviously refined and tend to become fine isometric crystals. The size of the eutectic Si decreases, and its shape is modified. The morphology and size of high temperature strengthening phases, such as Al_3CuNi, are optimized. The tensile properties of the alloy are improved at both room temperature and high temperature. However, with the addition of the Y element, the Al_2Si_2Y phase increases, and coarsening results in decreasing the strength of the alloy.

Author Contributions: Conceptualization, X.Q. and A.L.; methodology, X.Q.; investigation, X.Q.; formal analysis, X.Q.; writing—original draft, X.Q. and X.L.; funding acquisition, A.L.; resources, A.L.; supervision, A.L.; writing—review and editing, A.L.; data curation, X.L. All authors have read and agreed to the published version of the manuscript.

Funding: This research was funded by the 2021 Special funds for central guidance of local scientific and technological development funds, grant number GuiKeZY21195030; the Guangxi Key Research and Development Program, grant number GuiKeAB22080015; and the Specific Research Project of Guangxi for Research Bases and Talents, grant number GuiKeAD21238010.

Data Availability Statement: The original contributions presented in the study are included in the article; further inquiries can be directed to the corresponding author.

Conflicts of Interest: The authors declare no conflicts of interest.

References

1. Zhang, H.W.; Liu, Y.; Fan, T.X. Research Progress and Prospect of Casting Heat-resistant Aluminum Alloy. *Mater. Rev.* **2022**, *36*, 1–17.
2. Li, Q.S.; Li, A.M.; Sui, Q.P. Microstructure and High Temperature Creep Properties of ZrB2/Al-12Si Composites Prepared by in-situ Reaction Method. *Mater. Rev.* **2019**, *12–19*, 1–19.
3. Shyam, A.; Bahl, S. Heat-resistant aluminium alloys. *Nat. Mater.* **2023**, *22*, 425. [CrossRef] [PubMed]
4. Manasijevic, S.; Radisa, R.; Markovic, S.; Acimovic-Pavlovic, Z.; Raic, K. Thermal Analysis and Microscopic Characterization of the Piston Alloy AlSi13Cu4Ni2Mg. *Intermetallics* **2011**, *19*, 486–492. [CrossRef]
5. Zhang, S.H. Progress of Application of Aluminum Alloy in automobile. *Automot. Ind. Res.* **2003**, *3*, 36–39.
6. Sui, Y.D.; Wang, Q.D. Application Research and Development of cast Heat-resistant Aluminum Alloy in Engine. *Mater. Rev.* **2015**, *29*, 14–19.
7. Bi, J.; Liu, L.; Zhang, D.S.; Wang, H.X.; Zheng, L.Q.; Dong, G.J. Research Progress of casting, Quick-setting and Additive Heat-resistant Aluminum Alloys. *Chin. J. Non-Ferr. Met.* **2022**, 1–41.
8. Ram, S.C.; Chattopadhyay, K.; Chakrabarty, I. Microstructures and High Temperature Mechanical Properties of A356-Mg2Si Functionally Graded Composites in as-cast and Artificially aged (T6) Conditions. *J. Alloys Compd.* **2019**, *805*, 454–470. [CrossRef]
9. Zuo, L.; Ye, B.; Feng, J.; Zhang, H.; Kong, X.; Jiang, H. Effect of ε-Al3Ni Phase on Mechanical Properties of Al-Si-Cu-Mg-Ni Alloys at Elevated Temperature. *Mater. Sci. Eng. A* **2020**, *772*, 138794. [CrossRef]
10. Yang, Y.; Li, Y.; Wu, W.; Zhao, D.; Liu, X. Effect of Existing Form of Alloying Elements on the Microhardness of Al-Si-Cu-Ni-Mg Piston Alloy. *Mater. Sci. Eng.* **2011**, *528*, 5723–5728. [CrossRef]
11. Liu, Y.; Jia, L.; Wang, W.; Jin, Z.; Zhang, H. Effects of Ni Content on Microstructure and Wear Behavior of Al-13Si-3Cu-1Mg-xNi-0.6Fe-0.6Mn Alloys. *Wear* **2022**, *500*, 204365. [CrossRef]
12. Ghosh, A.; Manojit, G.; Gyan, S. On the Role of Precipitates in Controlling Microstructure and Mechanical Properties of Ag and Sn Added 7075 Alloys During Artificial Ageing. *Mater. Sci. Eng.* **2018**, *738*, 399–411. [CrossRef]
13. Qian, Z.; Liu, X.F.; Zhao, D.G.; Zhang, G.H. Effects of Trace Mn Addition on the Elevated Temperature Tensile Strength and Microstructure of a Low-Iron Al–Si Piston Alloy. *Mater. Lett.* **2008**, *62*, 2146–2149. [CrossRef]

14. Li, J.; Peng, Y.; Guo, X.; Liu, J.; Li, L.; Zhang, N.; Cui, X.; Wang, X.; Yuan, Z.; Lu, K. On the Microstructures and Properties of a Zr-modified Al-Si-Cu-Mg alloy at Intermediate Temperature. *J. Alloys Compd.* **2025**, *1010*, 178328. [CrossRef]
15. Emadi, D.; Rao, A.P.; Mahfoud, M. Influence of Scandium on the Microstructure and Mechanical Properties of A319 Alloy. *Mater. Sci. Eng.* **2010**, *527*, 6123–6132. [CrossRef]
16. Li, X.; Li, A.M.; Qin, X.D.; Yang, H.L.; Cheng, P. Effect of La on the Microstructures and Mechanical Properties of Al-5.4Cu-0.7Mg-0.6Ag Alloys. *Materials* **2024**, *17*, 4141. [CrossRef] [PubMed]
17. Lu, B.; Li, A.M.; Rao, Y.; Wang, L.; Zuo, T.; Hu, Y. Effect of Rare Earth Y and Heat Treatment on Microstructure and Properties of 6016 Aluminum Alloy. *Mater. Rev.* **2002**, *36*, 139–146.
18. Li, Q.; Zhang, Y.; Lan, Y.; Pei, R.; Feng, X.; Xia, T.; Liu, D. Effect of Scandium Addition on Microstructure and Mechanical Properties of as-cast Al-5%Cu alloys. *Vacuum* **2020**, *177*, 109385. [CrossRef]
19. Li, Q.L.; Li, B.Q.; Zhu, Y.Q. Modification of multi-component Al-Si Castingpiston Alloys by Adding of Rare Earth Yttrium. *Microsc. Microanal.* **2019**, 1–15.
20. Yu, S.R.; Yan, Z.J.; Xiong, W.; Yan, L. Study on Microstructure and Mechanical Properties of ZL107 Alloy Added with Yttrium. *J. Rare Earths* **2013**, *31*, 198–203. [CrossRef]
21. Jia, J.Y.; Chen, Z.Q.; Hu, W.X. Effect of La and Y on Microstructure of Refined A356 Aluminum Alloy. *Rare Earth* **2020**, *41*, 41–46.
22. Li, B.; Wang, H.W.; Jie, J.C.; Wei, Z.J. Effects of Yttrium and Heat Treatment on the Microstructure and Tensile Properties of Al–7.5Si–0.5Mg Alloy. *Mater. Des.* **2011**, *32*, 1617–1622. [CrossRef]
23. Nogita, K.; Yasuda, H.; Yoshiya, M. The role of trace element segregation in the eutectic modification of hypoeutectic Al-Si alloys. *J. Alloys Compd.* **2010**, *489*, 415–420. [CrossRef]
24. Sui, Y.D.; Wang, Q.D.; Wang, G.L.; Liu, T. Effects of Sr Content on the Microstructure and Mechanical Properties of Cast Al–12Si–4Cu–2Ni–0.8 Mg Alloys. *J. Alloys Compd.* **2015**, *622*, 572–579. [CrossRef]
25. Wan, B.; Chen, W.; Liu, L. Effect of Trace Yttrium Addition on the Microstructure and Tensile Properties of Recycled Al–7Si–0.3Mg–1.0Fe Casting Alloys. *Mater. Sci. Eng.* **2016**, *666*, 165–175. [CrossRef]
26. Song, Z.X.; Li, Y.D.; Liu, W.J.; Yang, H.K.; Cao, Y.J.; Bi, G.L. Effect of La and Sc Co-Addition on the Mechanical Properties and Thermal Conductivity of As-Cast Al-4.8% Cu Alloys. *Metals* **2021**, *11*, 1866. [CrossRef]
27. Wei, F.F.; Lei, Y.S.; Yan, H.; Xu, X.; He, J. Microstructure and Mechanical Properties of A356 Alloy with Yttrium Addition Processed by Hot Extrusion. *J. Rare Earths* **2019**, *37*, 659–667. [CrossRef]
28. Xiao, D.H.; Song, M.; Chen, K.H.; Huang, B.Y. Effect of Rare Earth Yb Additionon Mechanical Properties of Al–5.3Cu–0.8Mg–0·6Ag Alloy. *Mater. Sci. Technol.* **2007**, *23*, 1156–1160. [CrossRef]
29. Srivastava, N.; Chaudhari, G.P.; Qian, M. Grain Refinement of Binary Al-Si, Al-Cu and Al-Ni Alloys by Ultrasonication. *J. Mater. Proces. Technol.* **2017**, *249*, 367–378. [CrossRef]
30. Kumar, R.; Villanova, J.; Lhuissier, P.; Salvo, L. In Situ Nanotomography Study of Creep Cavitiesin Al-3.6-Cu Alloy. *Acta Mater.* **2019**, *166*, 18–27. [CrossRef]
31. Feng, J.; Ye, B.; Zuo, L.; Wang, Q.; Wang, Q.; Jiang, H.; Ding, W. Bonding of Aluminum Alloys in Compound Casting. *Metall. Mater. Trans. A* **2017**, *48*, 4636–4644. [CrossRef]
32. Yang, Y.; Zhong, S.Y.; Chen, Z.; Wang, M.; Ma, N.; Wang, H. Effect of Cr Content and heat-treatment on the High Temperature Strength of Eutectic Al–Si Alloys. *J. Alloys Compd.* **2015**, *647*, 63–69. [CrossRef]